Backbone Dynamics of an Oncogenic Mutant of Cdc42Hs Shows Increased Flexibility at the Nucleotide-Binding Site†

Paul D. Adams,‡ Adrienne P. Loh,§ and Robert E. Oswald*,‡

Department of Molecular Medicine, College of Veterinary Medicine, Cornell University, Ithaca, New York 14853, and Department of Chemistry, University of Wisconsin−LaCrosse, LaCrosse, Wisconsin 54601

Received May 5, 2004; Revised Manuscript Received June 8, 2004

ABSTRACT: Cdc42Hs, a member of the Ras superfamily of GTP-binding signal transduction proteins, binds guanine nucleotides, and acts as a molecular-timing switch in multiple signal transduction pathways. The structure of the wild-type protein has been solved (Feltham et al. (1997) *Biochemistry 36*, 8755−8766), and the backbone dynamics have been characterized by NMR spectroscopy (Loh et al. (1999) *Biochemistry 38*, 12547−12557). The F28L mutation of Cdc42Hs is characterized by an increased rate of cycling between the GTP and GDP-bound forms leading to cell transformation (Lin et al. (1997) *Curr. Biol. 7*, 794−797). Here, we describe the backbone dynamics of Cdc42Hs(F28L)-GDP using ^{1}H-^{15}N NMR measurements of T_1, $T_{1\rho}$, and steady-state NOE at two magnetic field strengths. Residue-specific values of the generalized order parameters (S_s^2 and S_f^2), local correlation time (τ_e), and exchange rate (R_{ex}) were obtained using the Lipari−Szabo formalism. Chemical-shift perturbation analysis suggested that very little structural change was evident outside of the nucleotide-binding site. However, residues comprising the nucleotide-binding site, as well as the nucleotide itself, exhibit increased dynamics over a wide range of time scales in Cdc42Hs(F28L) relative to the wild type. In addition to changes in dynamics measured by relaxation methods, hydrogen−deuterium exchange indicated a substantial disruption of the hydrogen-bonding network within the nucleotide-binding site. Thus, local dynamic changes introduced by a single-point mutation can affect important aspects of signaling processes without disrupting the conformation of the whole protein.

Cdc42Hs is a member of the Ras superfamily of proteins that are involved in a variety of cellular processes controlled by cycling between a biologically active GTP[1] form and an inactive GDP-bound form (*1*, *2*). GTP is hydrolyzed to GDP by the intrinsic GTPase activity of the protein; however, the cycle of binding, hydrolysis, and rebinding of the nucleotide is controlled by a number of regulatory proteins including guanine nucleotide exchange factors (GEFs), which catalyze nucleotide exchange (*3*, *4*); GTPase-activating proteins (GAPs), which stimulate hydrolysis (*5*); and guanine nucleotide dissociation inhibitors (GDIs), which inhibit GTP hydrolysis and GDP dissociation (*6*). Mutations in Cdc42Hs and other Ras proteins have been shown to lead to uncontrolled cell proliferation (*1*, *7*). In the case of Ras p21, mutations that inhibit the GTPase activity (e.g., G12V) are responsible for a number of types of cancer (*1*). Mutations in Cdc42Hs that increase the rate of cycling between the active and inactive forms are oncogenic (*8*).

Studies have shown that GTP-binding proteins, including Cdc42Hs, contain a nucleotide-binding region that is highly conserved. The nucleotide-binding site of H-Ras p21 has been described using X-ray crystallography (*9*). The bound nucleotide interacts with several regions of the H-Ras structure: Loop 1, residues 116−119, residues 145−147, and F^{28}. Loop 1 (P loop), which contains the consensus sequence ^{10}GXXXXGKST^{18}, interacts with the terminal phosphate group of the nucleotide. This sequence is found in most guanine nucleotide-binding proteins as well as a few adenine nucleotide-binding proteins (*10*). The nucleotide also interacts with residues 116−119, particularly with the hydrophobic portion of the side chain of a K^{117}. The sequence of residues 116−119 (^{116}NKXD^{119}) is well-conserved in GTP-binding proteins (*11*), although the sequence (but not the function) differs in the Rho proteins (^{115}TQXD^{118}). The residue at 116 forms a link to the Loop 1 region and residues 145−147 via hydrogen bonding. The residues ^{145}SAK^{147} in H-Ras appear to contribute to the nucleotide-binding pocket via hydrogen bonding with residues 116−119, and the hydrocarbon chain of K^{147} interacts with the aromatic side chain of F^{28} through hydrophobic interactions (because of the 13-residue insert

† This material is based on work supported by the National Science Foundation under a grant awarded to P.D.A. in 2002 and by a grant from the National Institutes of Health (R01 GM56223) to R.E.O.

* To whom correspondence should be addressed: Department of Molecular Medicine, College of Veterinary Medicine, Cornell University, Ithaca, NY 14853. Phone: (607) 253-3877. Fax: (607) 253-3659. E-mail: reo1@cornell.edu.

‡ Department of Molecular Medicine, Cornell University, Ithaca, NY 14853.

§ Department of Chemistry, University of Wisconsin−LaCrosse, La Crosse, WI 54601.

[1] Abbreviations: F28L, mutation of phenylalanine 28 in Cdc42Hs to leucine; GDP, guanosine-5′-diphosphate; GTP, guanosine-5′-triphosphate; GAP, GTPase-activating protein; GEF, guanidine exchange factor; GDI, guanidine nucleotide dissociation inhibitor; HSQC, heteronuclear single-quantum correlation; IPTG, isopropyl β-D-thiogalactopyranoside; Loop 1, residues 10−18 on Cdc42Hs; NMR, nuclear magnetic resonance; NOE, nuclear Overhauser effect; Switch I, residues 31−40 on Cdc42Hs; Switch II, residues 57−74 on Cdc42Hs; Insert region, residues 118−134 on Cdc42Hs; T_1, longitudinal relaxation time; T_2, transverse relaxation time; $T_{1\rho}$, transverse relaxation time in the rotating frame; S^2, generalized order parameter; τ_e, local correlation time; τ_m, molecular or global correlation time; R_{ex}, chemical exchange rate.

10.1021/bi0490901 CCC: $27.50 © 2004 American Chemical Society
Published on Web 07/15/2004

region (122−134) unique to Cdc42Hs and other Rho proteins, the corresponding region in Cdc42Hs is ^{158}SAL^{160}). Despite these other interactions, F^{28} is the principal stabilizer of the nucleotide in these proteins via a strong interaction with the aromatic ring of the bound nucleotide (*12*−*14*). ^{31}P NMR studies on the single-point mutant of H-Ras p21, F28L, showed significant chemical-shift changes for the GDP-bound mutant relative to the wild-type protein (*14*). In addition, the GDP dissociation rate increased by more than 28-fold in the F28L mutant (*14*, *15*). These findings suggest that F^{28} is an important contributor to the stability of GDP binding in H-Ras p21, as well as other Rho proteins, including Cdc42Hs.

NMR spectroscopy provides an excellent way to probe for correlations between the structure, dynamics, and function of proteins (*16*). Dynamics studies have provided valuable information on structure−function relationships in a variety of protein systems (*17*−*24*). Intramolecular motions may be crucial for many aspects of protein functions including regulatory control (*25*, *26*). In this paper, we present a detailed analysis of the backbone dynamics of the single-point mutant of Cdc42Hs, Cdc42Hs(F28L). This mutation results in cell transformation that is thought to be a result of decreased affinity for the nucleotide and an increased rate of cycling between the GDP and the GTP-bound forms (*8*). An analysis of the ^{1}H-^{15}N NMR backbone relaxation measurements of Cdc42Hs(F28L) in comparison to those of the wild-type protein (*21*) indicates how the mutation disrupts interactions that destabilize the local structure, leading to multiple time-scale motions of residues in the binding site.

EXPERIMENTAL PROCEDURES

Protein Expression and Purification. A Cdc42Hs construct with a C-terminal truncation (*27*) was used to prepare the F28L mutation. The construct was cloned into a pET-15b vector and subsequently overexpressed in *Escherichia coli*. Cultures (5 mL) were initially grown to saturation and used to seed 1- or 2-L cultures grown in minimal media containing ^{15}N-NH_4Cl as the sole nitrogen source. The cultures were grown at 37 °C to an OD_{560} of 0.4−0.6, and expression was induced by adding 1 mM IPTG (isopropyl β-D-thiogalactopyranoside) for 7−12 h. The ^{15}N-labeled Cdc42Hs(F28L) was expressed as a His-tagged protein, and after expression, the protein was purified by column chromatography as previously described for Cdc42Hs (*27*), except that 1 mM Mg^{2+} was maintained in all solutions. The Mg^{2+} aided in preventing denaturation of the protein before completion of purification. After purification, the molecular weight of the protein was confirmed by MALDI mass spectrometry, and gel electrophoresis was used to check the purity of the protein sample. All buffer solutions were at pH 8 until the final stage of purification when the pH of the NMR sample buffer was reduced to 5.5. Cdc42Hs(F28L) was expressed in the GDP-bound (inactive) form. For dynamics studies using ^{15}N-labeled GDP, unlabeled Cdc42Hs wild-type and Cdc42Hs(F28L) samples were prepared as described above, except that natural abundance NH_4Cl was used, and 0.1 mM ^{15}N-GDP was incorporated in all buffers throughout purification.

NMR Spectroscopy. All protein samples were prepared in an NMR sample buffer solution containing 25 mM NaCl, 10 mM NaH_2PO_4, 5 mM $MgCl_2$, and 1 mM NaN_3 with 8% D_2O at pH 5.5 (not adjusted for isotope effect) at Cdc42Hs(F28L) concentrations of 0.2−0.4 mM. NMR spectra were obtained using Varian Inova 600 and 500 MHz spectrometers. Both spectrometers were equipped with triple-resonance pulsed-field-gradient probes. All NMR spectra were acquired at 25 °C in States-TPPI mode for quadrature detection (*28*). Carrier frequencies for ^{1}H and ^{15}N were 4.77 and 115.9 ppm, respectively. ^{15}N T_1 and $T_{1\rho}$ values were measured at 500 and 600 MHz using 128 × 512 real data points at 16 scans per point using the pulse sequences provided by Kay et al. (*29*), with 12 delays for T_1 of 12−1100 ms and 8−100 ms for $T_{1\rho}$. The spin lock field strength for $T_{1\rho}$ was 2.5 kHz. Steady-state heteronuclear ^{1}H-^{15}N NOE values were also measured at 500 and 600 MHz and acquired using 128 × 512 real data points with 16 scans per point. Hydrogen−deuterium exchange was assessed by lyophilizing the sample and resuspending in 100% D_2O. A series of ^{1}H-^{15}N HSQC experiments were performed, and the decrease in the volume and eventual disappearance of ^{1}H-^{15}N cross peaks were used to determine the extent of exchange of deuterons for protons.

NMR spectra were processed using NMRPipe version 1.6 (*30*). The spectra were zero-filled and then apodized using a Gaussian window function prior to Fourier transformation. After Fourier transformation, a baseline correction was applied. Peaks were assigned using the PIPP suite of programs (*31*). Peak volumes were calculated using the nonlinear least-squares fitting program, nlinLS (*30*). Values of the relaxation times T_1 and $T_{1\rho}$ were obtained using conjugate-gradient minimization and Monte Carlo simulations to fit the relaxation data points to an exponential decay function (*32*). The errors in the relaxation times, which were expressed as standard deviations, were chosen as the larger of those from the exponential fit or from the replicate sets of the measured relaxation delay points. T_2 values were calculated by correction for off-resonance effects of $T_{1\rho}$ as described previously (*21*). Individual NOE values were measured by calculating the ratio of the peak volumes of cross peaks according to

$$\mathrm{NOE} = \frac{V_{\mathrm{sat}}}{V_{\mathrm{nosat}}} \tag{1}$$

where V_{sat} and V_{nosat} are peak volumes measured with and without proton saturation, respectively. Three sets of each type of data (with and without proton saturation) were obtained. All nine possible ratios were used to calculate the final NOE values, and the standard deviation of the data set was used as the error in the NOE measurements.

Data Analysis. The measured relaxation parameters T_1, T_2, and NOE are related to the spectral density function [$J(\omega)$] through the order parameters (S^2) and local correlation times (τ_e) as described by Lipari−Szabo (*33*, *34*) and extended by Clore et al. (*35*)

$$J(\omega) = \frac{2}{5}\left[\frac{S^2\tau_m}{1+(\omega\tau_m)^2} + \frac{(1-S_f^2)\tau'_f}{1+(\omega\tau'_f)^2} + \frac{(S_f^2-S^2)\tau'_s}{1+(\omega\tau'_s)^2}\right] \tag{2}$$

where

$$\frac{1}{\tau'_i} = \frac{1}{\tau_i} + \frac{1}{\tau_m} \quad (3)$$

and ω is the Larmor frequency of the ^{15}N nucleus, τ_m is the global-tumbling time, τ_i is the local correlation time that describes motion on either a fast (f) or slow (s) time scale relative to that of τ_m ($\tau_f < \tau_s < \tau_m$), and $S^2 = S_f{}^2 S_s{}^2$ is the generalized order parameter, where $S_f{}^2$ and $S_s{}^2$ are the amplitudes that describe motions on fast and slow time scales, respectively. S^2 ranges from 1 representing rigid or restricted motion to 0 representing isotropic motion. As described by Mandel et al. (*36*), four simpler models of the spectral density function were also considered in the data analysis (Table 1). Model 1 includes motion for which the time scale is too fast to measure; model 2 includes an explicit correlation time; and models 3 and 4 are equivalent to models 1 and 2 with a term for chemical exchange. The value of τ_m for Cdc42Hs(F28L) was calculated from a grid search using a filtered average value of T_1/T_2 measured at 500 and 600 MHz (*37*). Assuming an isotropic model for Cdc42Hs(F28L) as determined for the wild-type protein (*21*), values of the dynamics parameters characterizing residue-specific dynamics were obtained by fitting the relaxation data at both field strengths to five standard models based on eq 2 (Table 1) using ModelFree (version 4) (*38*). For each model, 300 data sets were generated from the experimental relaxation data points with a Gaussian distribution of experimental errors. The quality of the fits was evaluated using a χ^2 comparison of the experimental and calculated relaxation parameters, and the motional model that best fit the data was chosen according to methods outlined previously (*21*), using an *F* test criterion.

Table 1: Dynamic Models Used to Fit Experimental Relaxation Data to the Extended Lipari−Szabo Formalism (*33*−*35*)

model	fit parameters	assumptions
1	S^2	$S_s^2 = 1$, $R_{ex} = 0$
2	S^2 and τ_e	$S_s^2 = 1$, $\tau_e < \tau_m$, $R_{ex} = 0$
3	S^2 and R_{ex}	$S_s^2 = 1$,
4	S^2, τ_e, and R_{ex}	$S_s^2 = 1$, $\tau_e < \tau_m$
5	S_f^2, S_s^2, and τ_e	$\tau_e < \tau_m$, $R_{ex} = 0$

RESULTS

Backbone Assignments. An overlay of the ^1H-^{15}N HSQC spectrum of Cdc42Hs(F28L)-GDP on the wild-type Cdc42Hs-GDP spectrum is shown in Figure 1A. The chemical shifts of the majority of the resonances were unchanged (parts A and B of Figure 1). The previous sequential assignments for the Cdc42Hs-GDP construct (*39*) and the ^{15}N-separated NOESY and TOCSY spectra of Cdc42Hs(F28L) were used to assign backbone amide proton/nitrogen resonances, resulting in assignments for 142 cross peaks of the mutant protein compared to 143 assignments for the wild type. Interestingly, significant chemical-shift differences were observed between Cdc42Hs(F28L) and the wild type in regions involving the nucleotide-binding site: the Loop 1 region (residues 10−18), residues 158−160, and L^{28}.

Hydrogen−Deuterium Exchange. Flexibility on a slow time scale was studied by NMR hydrogen−deuterium exchange experiments. The results of the experiment are outlined along with the sequences of the constructs in Figure 2. As was the case with the chemical shift data, the wild-type and mutant proteins exhibited similar H−D exchange behavior for most of the protein. However, there were some noticeable differences for residues comprising the nucleotide-binding site (residues 10, 12, 15−18, 116, 118, 158, and 160), which were shielded from the solvent in the wild type but were fully or nearly fully exchanged in Cdc42Hs(F28L) after only 5 min in D_2O.

Relaxation Data. The average backbone relaxation parameters (T_1, T_2, and NOE) for Cdc42Hs(F28L)-GDP are compared to those obtained from wild-type Cdc42Hs-GDP (*21*) at 500 and 600 MHz in Table 2, and relaxation parameters for Cdc42Hs(F28L) are shown in parts A−C of Figure 3. Because the concentrations of the two proteins are different, relaxation parameters cannot be directly compared because the global-tumbling times are different (see below). However, in comparison to the average behavior of the molecule, some differences in the relaxation parameters are apparent in the nucleotide-binding site of Cdc42Hs(F28L) versus the wild-type protein. In the Loop 1 region of Cdc42Hs(F28L) (residues 10−18), T_1 values are higher than the average T_1, with little variation in T_1 over the rest of the protein. In contrast, very little variation in T_1 was observed across the entire wild-type protein (*21*). The Loop 1 region also shows a decrease in T_2 from the average T_2 value for Cdc42Hs(F28L), whereas in the wild type, the Loop 1 T_2 values do not deviate from the average. Residues 115−118 show a slight decrease in T_2 with respect to the average T_2 value of the protein in Cdc42Hs(F28L), but this is similar to the T_2 behavior of the corresponding residues in the wild type. Residue L^{28} in Cdc42Hs(F28L) shows an increased T_2 relative to the rest of the protein. F^{28} also shows this trend in T_2 in the wild-type; however, the deviations are much less significant for F^{28} in the wild type than that for L^{28}. The T_2 behavior of residues 158−160 was similar in both proteins; however, there was a drop in the NOE values relative to the average in Cdc42Hs(F28L).

The relaxation behavior of ^{15}N-GDP bound to the natural abundance Cdc42Hs wild type and Cdc42Hs(F28L) (with both proteins at the same concentration) was also measured (Table 3). ^{15}N-GDP in Cdc42Hs(F28L) shows a ∼1.3-fold decrease in T_1, ∼1.5-fold increase in T_2, and >2-fold decrease in NOE relative to ^{15}N-GDP in the wild type. Overall, the backbone and nucleotide relaxation parameters show that (1) relaxation measurements for the F28L mutant in or near the nucleotide-binding site suggest increased motion relative to the ^{15}N-GDP wild type and that (2) the nucleotide in Cdc42Hs(F28L) exhibits increased motion relative to the nucleotide in the wild type as shown by the distinct increase in T_2 and decrease in NOE (*40*).

Backbone Dynamics. Residue-specific dynamics parameters S^2, τ_e, and R_{ex} and the global dynamics parameter τ_m for Cdc42Hs(F28L) were obtained by fitting the relaxation data at both field strengths to five different dynamics models of the extended Lipari−Szabo modelfree formalism (Table 1), assuming isotropic global tumbling (*21*). Values of $S_{avg}{}^2$ and τ_m for the two constructs are shown in Table 4. Also given are differences in S^2 between the mutant and wild type in the nucleotide- and effector-binding regions. The differences in τ_m between the two protein samples are attributed to the more dilute concentrations of Cdc42Hs(F28L) (0.2−0.3 mM) versus the concentration (0.9 mM) used for the wild type (*21*). A decreased concentration usually results

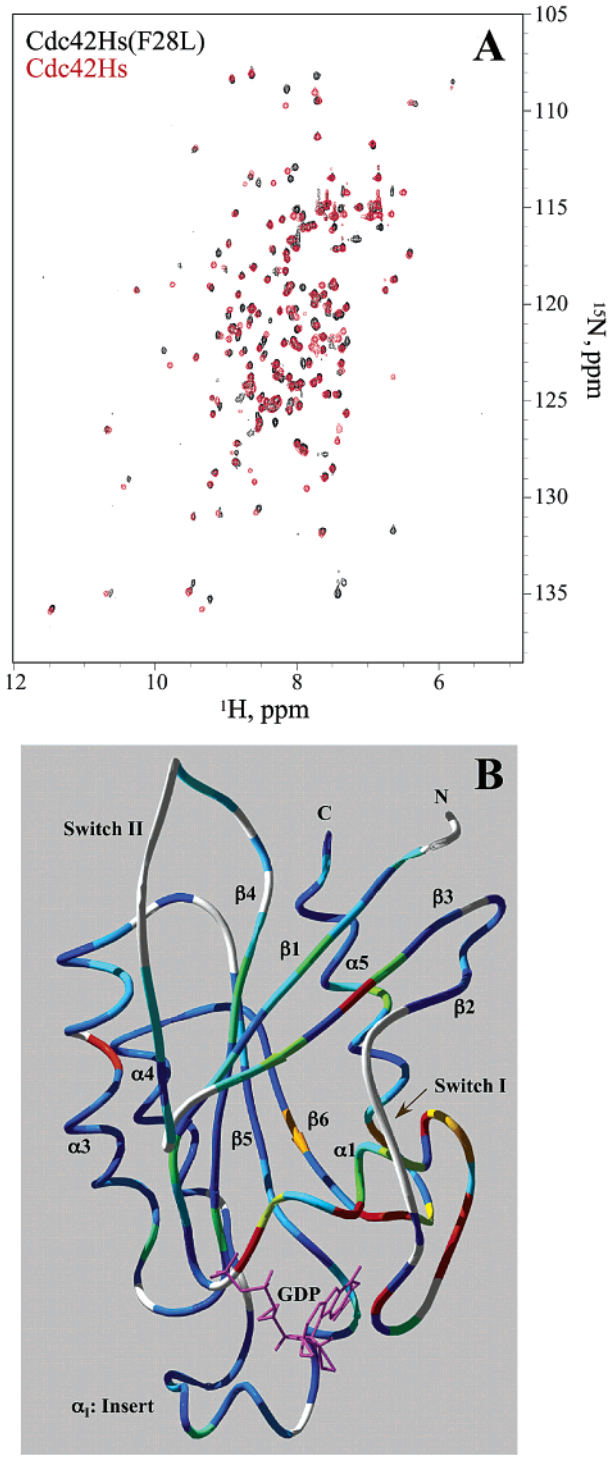

FIGURE 1: Chemical-shift perturbation arising from the F28L mutation. (A) Overlay of ^{1}H-^{15}N HSQC experiments of ^{15}N-labeled wild-type Cdc42Hs-GDP (red) and ^{15}N-labeled Cdc42Hs(F28L)-GDP (black) at 500 MHz. (B) Solution structure of Cdc42Hs [1AJE (*39*)] indicating chemical-shift changes in Cdc42Hs(F28L) relative to wild-type Cdc42Hs: white ($\gamma = 0$), blue−cyan ($0 < \gamma \leq 1.5$), cyan−green ($1.5 < \gamma \leq 2.5$), green−yellow ($2.5 < \gamma \leq 3.5$), yellow−red ($3.5 < \gamma \leq 4.5$), red ($\gamma > 4.5$), where $\gamma = \sqrt{(\Delta H/0.03)^2+(\Delta N/0.3)^2}$.

in a faster tumbling time because of the decreased viscosity of the solution. For each residue in Cdc42Hs(F28L), the model describing the motion of the N−H bond vector was chosen as the one that produced the best fit between the experimental and calculated values of the relaxation parameters. The model assignments for Cdc42Hs(F28L) are compared to the assigned models for the wild type in parts A and B of Figure 5. For eight residues in Cdc42Hs(F28L) (residues 57, 58, 72, 75, 80, 113, 127, and 178), the value of τ_e approached the value of τ_m (considered the upper bound of motion) or the error in τ_e was 80−110%. In these cases, it was concluded that the local motions in these residues were either too difficult or complex to model accurately.

In comparing the overall dynamics for Cdc42Hs(F28L) to that of the wild type, a clear difference in the values of S_{avg}^2 between the proteins was evident. The dynamics parameters generated for the wild type (*21*) were calculated using NOE data at only one field strength (600 MHz), whereas for Cdc42Hs(F28L), the dynamics analysis was performed using NOE data at two field strengths. In addition, error estimates in the NOE data for the wild type were determined from the rms baseline noise (*41*), whereas for Cdc42Hs(F28L), the error estimates in the NOE data were calculated from the standard deviation of all permutations of the ratio of peak volumes from triplicate measurements of peak intensities in the presence and absence of proton saturation. Also, anomalous measurements of V_{sat} or V_{nosat} could be identified from the triplicate data sets for Cdc42Hs(F28L), which was not possible for the wild type. In an attempt to interpret the differences in S^2, we repeated dynamics calculations for Cdc42Hs(F28L) using the calculated T_1 and T_2 relaxation parameters and (1) only 600 MHz NOE data, (2) modifying the error estimates in the 600 MHz NOE data to be on the order of the magnitudes of the error estimates in the NOE data for the wild type and rerunning the simulation of Cdc42Hs(F28L) using only 600 MHz NOE data, and (3) modifying the error estimates in both the 600 and 500 MHz NOE data to be on the order of the deviations in the NOE data for the wild type and rerunning the simulation of Cdc42Hs(F28L) using both NOE data sets. Under all three conditions, the S^2 values of Cdc42Hs(F28L) remained virtually unchanged. Thus, the discrepancy in S_{avg}^2 is probably due to the differences in the way the NOEs were calculated. It is known that NOE is sensitive to S^2, provided that the overall tumbling time for the protein is >10 ps (*32*). However, it should not be discounted that the difference in S^2 between the proteins might in fact be due to a greater amplitude of motion for all residues in Cdc42Hs(F28L) versus the wild type. This possibility seems unlikely because the S^2 profile is similar for both proteins [except for Loop 1 in Cdc42Hs(F28L), where the values were uniformly lower throughout the region; Figure 4] and the models used to fit a majority of the residues in both proteins are similar (Figure 5).

As was the case with the relaxation parameters, the nucleotide-binding regions show some interesting deviations in their dynamics behaviors. Values of S^2 for several residues in Loop 1 of Cdc42Hs(F28L) are significantly decreased relative to the mean S^2 value of the protein, indicating a greater amplitude of internal motion for these residues in the binding region (Table 4). In addition, residues 10 and 13−18 were best fit by models 3 or 4, both of which contain a chemical-exchange term (Figure 4). In contrast, all of the residues of the Loop 1 region (10−18) of the wild type obey model 1 dynamics with $S^2 > 0.9$ with the exception of residue 16, and S^2 in this region deviates only slightly from the average S^2 for the wild-type protein. The chemical

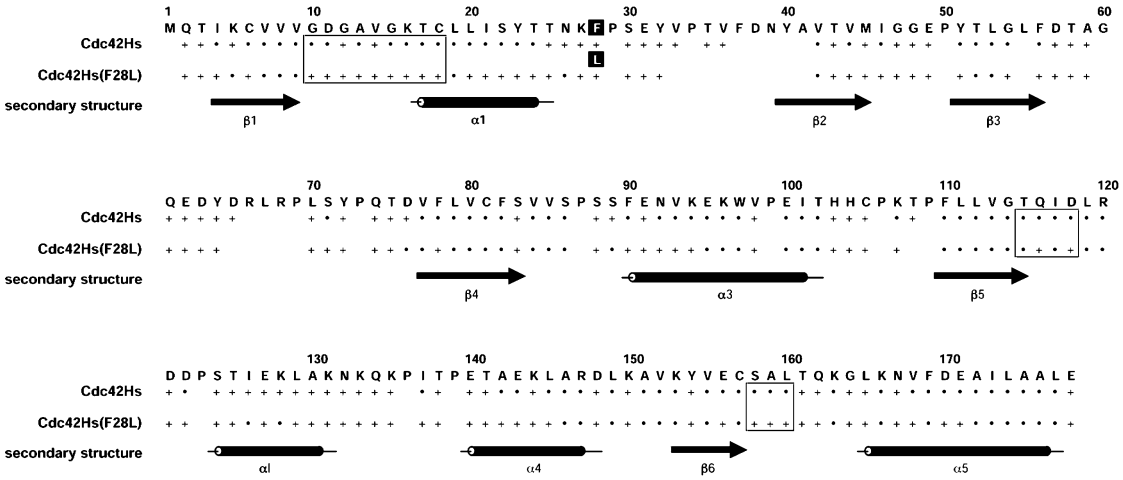

FIGURE 2: Sequence of Cdc42Hs showing the position of the F28L mutation. Also shown is the hydrogen−deuterium exchange data. A filled circle indicates that the exchange of the amide proton in D_2O had an exchange half-life of greater than 1 h, and a plus sign indicates that an exchange was complete within 5 min. If the exchange could not be determined because of the overlap or a weak signal, the column was left blank. The secondary structure from solution NMR (*39*) is also shown.

Table 2: Average Backbone Relaxation Parameters for Cdc42Hs(F28L)-GDP and Cdc42Hs-GDP (Wild Type)[a]

	T_1 (s)		T_2 (s)		NOE	
construct	500 MHz	600 MHz	500 MHz	600 MHz	500 MHz	600 MHz
Cdc42Hs(F28L)-GDP	0.71 ± 0.06	0.99 ± 0.05	0.073 ± 0.003	0.068 ± 0.003	0.77 ± 0.06	0.80 ± 0.06
Cdc42Hs-GDP[b]	0.72 ± 0.07	1.05 ± 0.02	0.053 ± 0.002	0.049 ± 0.001		0.76 ± 0.02

[a] Concentration for Cdc42Hs(F28L) was 0.2 mM, and concentration for Cdc42Hs (wild type) was 0.8 mM. [b] Data from Loh et al. (*21*).

exchange and lowered order parameters indicate a significant increase in motion as a result of the L^{28} mutation. The value of S^2 for L^{28} also drops significantly (~29%) below the mean value of S^2 for the Cdc42Hs(F28L) protein. This finding is consistent with the observed increase in T_2 and decrease in NOE for the residue, indicating a reduced order. L^{28} was best fit by model 5, which includes complex motion on fast and slow time scales. The order parameter for F^{28} in Cdc42Hs-GDP was similar to the mean value of S^2 for the protein and was also best fit by model 5. The different S^2 values for the residues at position 28 in the two proteins clearly indicate a greater amplitude of motion for L^{28} in the mutant protein. Residues 115−118 and residues 158−160 directly facilitate the stabilization of the nucleotide-binding site in Cdc42Hs through interactions with the guanine nucleotide ring. The values of S^2 for residues 115−118 and 158−160 in Cdc42Hs(F28L) show similar dynamics character to the corresponding residues in the wild type, with negligible differences in S^2 in these regions for both proteins relative to the bulk molecule. The model comparisons between the two proteins in these regions are also essentially identical. However, there are two residues in the region comprising 115−118 (Q^{116} and I^{117}) that have noticeably decreased S^2 values relative to the average S^2 for Cdc42Hs(F28L), which was not seen in the wild type.

DISCUSSION

The single-point mutation of F28L in Cdc42Hs introduces several differences in flexibility at or near the nucleotide-binding site, with few differences elsewhere. The most pronounced results are (1) a significant difference in the amplitude of motion for L^{28} versus F^{28}, (2) increased chemical exchange and a significant decrease in S^2 in Loop

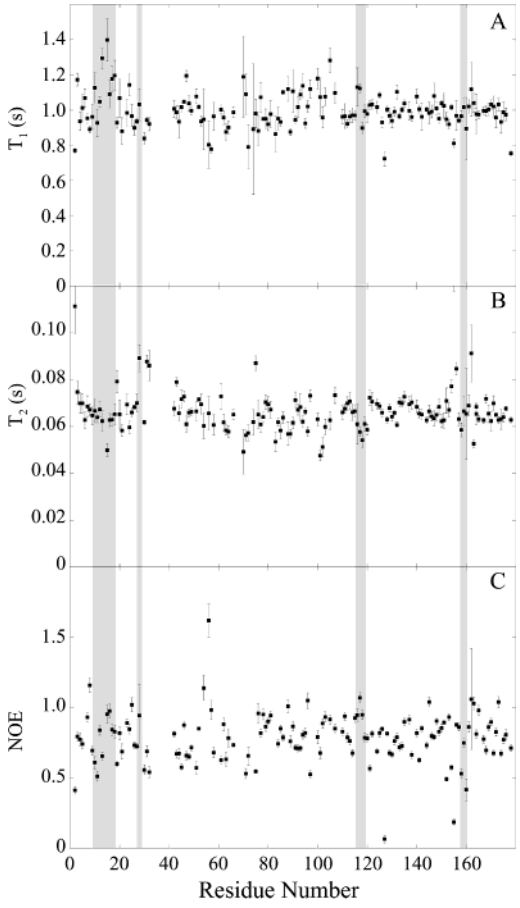

FIGURE 3: Relaxation data for Cdc42Hs(F28L) measured at 600 MHz. The shaded bars indiate the nucleotide-binding regions (residues 10−18, 28, 115−119, and 158−160). (A) T_1, (B) T_2, and (C) NOE.

Table 3: Relaxation Parameters of the ^{15}N-GDP Nucleotide in Cdc42Hs Constructs[a]

construct	T_1 (s)	T_2 (s)	NOE
Cdc42Hs(F28L)-GDP	0.67 ± 0.08	0.063 ± 0.003	0.38 ± 0.07
Cdc42Hs-GDP	0.85 ± 0.05	0.045 ± 0.003	0.81 ± 0.18

[a] Concentration of both constructs was 0.4 mM.

Table 4: Average Values of the Overall Order Parameters, Deviations from the Average S^2 (ΔS^2),[a] and Global Correlation Times (τ_m) for Cdc42Hs(F28L)-GDP and Cdc42Hs-GDP (Wild Type)[b]

	construct	
	Cdc42Hs(F28L)	Cdc42Hs
τ_m	12.2 ns	14.8 ns
average S^2	0.871 ± 0.005	0.952 ± 0.010
$\%\Delta S^2$ (28)	29%	0.5%
$\%\Delta S^2$ (10−18)	12%	1.7%
$\%\Delta S^2$ (115−118)	1.0%	0.9%
$\%\Delta S^2$ (158−160)	4.5%	3.3%
$\%\Delta S^2$ (Switch I)	1.0%	14%
$\%\Delta S^2$ (Switch II)	3.1%	0.2%
$\%\Delta S^2$ (Insert)	0.1%	0.2%

[a] $\%\Delta S^2 = |({}^{avg}S^2_{protein} - {}^{avg}S^2_{region})/{}^{avg}S^2_{protein}| \times 100$. [b] Region of the protein over which the order parameter is averaged is indicated in parentheses after $\%\Delta S^2$.

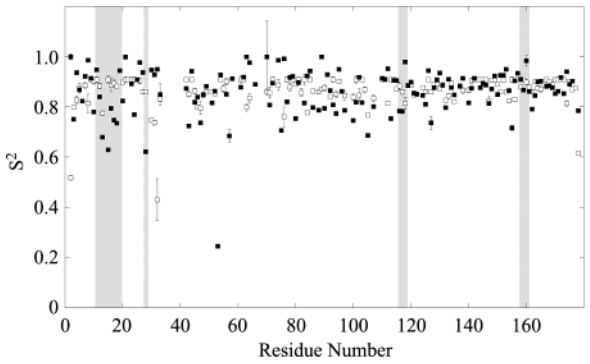

FIGURE 4: S^2 extracted using the extended Lipari−Szabo modelfree formalism for Cdc42Hs(F28L) (■) and wild-type Cdc42Hs (□). Because of systematic differences in the value of S^2 for the wild type, the S^2 values for the wild type were offset such that the average S^2 was equal to that of Cdc42Hs(F28L). The shaded bars indiate the nucleotide-binding regions (residues 10−18, 28, 115−119, and 158−160). For residues fit by model 5, $S^2 = S_f^2 S_s^2$.

1 (residues 10−18), (3) increased H−D exchange in Loop 1, residues 115−118, and residues 158−160, and (4) differences in relaxation parameters for the nucleotide itself. Likewise, NMR (*14*) and X-ray studies (*42*, *43*) on mutations in the nucleotide-binding site (positions 10 and 12) in H-Ras proteins have revealed only local perturbations of the structure of the protein immediately adjacent to the site of the mutation. The results of these studies suggest that the functional changes as a consequence of the F28L mutation are likely to be solely the result of modifications in the interactions involving the nucleotide and not a result of changes in effector-binding regions of the protein (Table 4). Here, we provide a detailed analysis of the localized dynamic changes introduced by the single-point mutation, seemingly without disrupting the structure of the entire protein, and discuss the impact of the observed increased backbone dynamics in regions of the nucleotide-binding site on the rapid cycling rate between GDP and GTP in Cdc42Hs(F28L).

Leucine 28. Solution (*39*) and crystal structures of Cdc42Hs (*44*), as well as other Ras proteins (*9*, *14*, *45*), show an orientation of the nucleotide with F^{28} that allows for a stabilizing overlap between the π orbitals of the nucleotide and the aromatic ring of the amino acid. This interaction is lost when L is substituted for F. In Cdc42Hs(F28L), S^2 for L^{28} is ∼29% lower than the average, while in Cdc42Hs, the S^2 for F^{28} is indistinguishable from the average. This indicates an increased amplitude of local motion for L^{28} relative to F^{28}. Interestingly, both L^{28} and F^{28} are best fit to models showing motion on two time scales (model 5). This suggests that both F^{28} and L^{28} exhibit complex motions on the pico- to nanosecond time scale but suggests that, in the wild type, these motions are low-amplitude because of the interaction between the side chain of F^{28} and the aromatic ring of the nucleotide.

The higher amplitude motions of L^{28} allow the nucleotide to be more flexible in the binding site. X-ray studies of Cdc42Hs show that the aromatic ring of F^{28} is also stabilized through a hydrophobic interaction with L^{160}. Similar hydrophobic contacts are seen between the corresponding residues in H-Ras proteins (*9*, *46*). The 3-D ^{1}H-^{15}N-NOESYHSQC spectrum of wild-type Cdc42Hs-GDP indicates close contacts between residues comprising the nucleotide-binding site and several residues adjacent to and including F^{28} (*39*). These include contacts between the amide proton of N^{26} and Hβ of A^{159}, the amide proton of F^{28} and Hδ of L^{160}, and amide protons of S^{30} and L^{160}. In contrast, for Cdc42Hs(F28L), the corresponding spectrum shows only one relatively weak NOE between the amide protons of L^{28} and L^{160}, indicating a disruption of interactions between the L^{28} region and residues 158−160, presumably contributing to the destabilization of the nucleotide-binding site in the mutant protein (Adams and Oswald, unpublished data).

Loop 1 Region (10−18). As in most GTP-binding proteins (*45*−*48*), residues 13−18 of the Loop 1 region interact with the phosphate groups of the nucleotide via hydrogen bonding. Residues G^{10} and G^{12} are highly conserved and are essential to the proper functioning the Rho GTP-binding proteins (*7*, *49*). Substitutions of G^{12} (e.g., G12V) abolish GTPase activity and lead to cell transformation in H-Ras (*49*) and Cdc42Hs (*50*). However, the structure of neither H-Ras(G12V) nor Cdc42Hs(G12V) shows global changes in the protein, with the structural modifications specifically localized to the site of the mutation (*42*, *43*, *46*, *51*). Furthermore, the crystal structure of Cdc42Hs-GDP shows that K^{16} interacts with the carbonyls of the glycine residues to help stabilize the Loop 1 region with the bound nucleotide (1AN0), similar to stabilizing interactions found in this region of H-Ras (*9*, *52*). Clearly, the Loop 1 residues are intimately involved in nucleotide binding. In Cdc42Hs(F28L), S^2 is 12% lower in Loop 1 relative to the average, indicating an increase in the amplitude of motion for these residues. Most residues in this region are best fit by models exhibiting chemical exchange (model 3 dynamics for residues 10 and 13−18 and model 4 dynamics for residue 16). The corresponding residues of Loop 1 in wild-type Cdc42Hs are all fit to a simple motional model (model 1), with only A^{13} showing chemical exchange (model 4). In addition, the values of S^2 for these residues in the wild type (*21*) do not deviate significantly from the average (Table 4). Furthermore, more residues exhibited H−D exchange in Cdc42Hs(F28L) than that in the wild type.

In wild-type Cdc42Hs, the backbone amide protons of residues 13−18 are shielded from the solvent (*39*), presumably, at least in part, because of hydrogen bonding with the phosphate groups of the nucleotide. For example, the crystal structure of Cdc42Hs shows that the main chain NH's of residues 15 and 18 hydrogen-bond with the α-phosphate group (1AN0). In Cdc42Hs(F28L), all amide protons exchanged with the solvent within the first 5 min of deuterium exposure. The observation of chemical and H−D exchange for the residues in this region indicate a significant increase in motion in the Loop 1 region over a wide range of time scales. Thus, it seems likely that the L^{28} mutation causes a conformational disruption of these residues such that there is an opening up of the nucleotide-binding site in Cdc42Hs(F28L), resulting in lost interactions between the nucleotide phosphate groups and Loop 1 and increased dynamics in this region.

Residues 115−118 and 158−160. The ^{115}TQID^{118} residues in Cdc42Hs are thought to behave similarly to the conserved motif found in Ras proteins, ^{116}NKXD^{119} (*9*, *11*). In Cdc42Hs, the amide protons of ^{115}TQID^{118} are involved in hydrogen-bonding networks that facilitate interactions with two other regions directly involved in the nucleotide-binding site: Loop 1 and residues 158−160. In addition, the hydrophobic portion of the side chain of Q^{116} interacts with the nucleotide base on the opposite side of F^{28}. The side chain of D^{118} forms a hydrogen bond with the N1-H of the nucleotide base, and the backbone amide proton of D^{118} forms a hydrogen bond with residues of the side chain of S^{158}. Hydrogen-bonding networks in residues 158−160 also play a crucial role in the stabilization of the nucleotide-binding site in Cdc42Hs, with the amide protons of residues 159 and 160 forming hydrogen bonds with the carbonyl oxygen of the nucleotide base. Also, the side chain of L^{160} packs with the phenyl ring of F^{28}, contributing to the stabilizing interaction between F^{28} and the nucleotide base.

Residues 115−118 and 158−160 in Cdc42Hs facilitate the stabilization of the nucleotide-binding region. Only small chemical-shift differences [Cdc42Hs(F28L) relative to the wild type] were observed for residues 115−118, but residues 158−160 showed significant changes. In addition, residues 115−118 in Cdc42Hs(F28L) and the wild-type protein are fit to similar motional models on the micro- to millisecond time scale (chemical exchange; Figure 5), and ΔS^2 for this region is the same for both proteins (Table 4). In Cdc42Hs(F28L) and the wild type, residues 158−160 all exhibit model 1 dynamics. However, the H−D exchange differs between the wild type and Cdc42Hs(F28L) for both regions. In the wild type, the backbone amide protons of all residues in these two regions are protected from exchange over several days, whereas in Cdc42Hs(F28L), the backbone amide protons of Q^{116}, D^{118}, and residues 158−160 are all exchanged within 5 min. This solvent exposure of residues in the nucleotide binding site of Cdc42Hs(F28L) may suggest that the hydrogen bonds are weaker and/or that the more water molecules can enter the binding site perhaps because of a looser packing that results from the mutation.

Nucleotide. Relaxation measurements performed on Cdc42Hs(F28L)-^{15}N-GDP and Cdc42Hs-^{15}N-GDP provide clear evidence of the increased motion of the nucleotide in Cdc42Hs(F28L) with respect to the wild type. The N1 proton of the nucleotide in the wild-type complex has a chemical shift of 12.81 ppm versus 12.92 ppm in the Cdc42Hs(F28L) complex. This downfield shift of the N1-H resonance in the nucleotide bound to Cdc42Hs(F28L) indicates a more polar chemical environment, suggesting that the nucleotide is more exposed to the solvent or some other polar/electron-rich group (*53*, *54*). The ^{1}H-^{15}N-NOESYHSQC spectrum of Cdc42Hs-^{15}N-GDP shows several NOE cross peaks between the nucleotide N1 proton and residues 119 and 160 that were not evident in the corresponding spectrum of Cdc42Hs(F28L)-^{15}N-GDP (data not shown), consistent with the looser packing or increased dynamics of the nucleotide-binding site. Samples of ^{15}N-GDP complexed with the wild-type and Cdc42Hs(F28L) proteins were prepared in equimolar concentrations, allowing the direct comparison of the relaxation data for the nucleotide in both proteins. The value of τ_m can be determined from the ratio of T_1/T_2, provided T_2 is not shortened by chemical exchange (*55*). Because dynamics parameters for the nucleotide were not calculated because relaxation parameters were acquired at only one field strength, chemical exchange cannot be confirmed or ruled out for the nucleotide. However, the ratio of T_1/T_2 for N1 of the nucleotide provides a way of estimating the degree of motion of the nucleotide alone. The T_1/T_2 ratio for Cdc42Hs(F28L)-^{15}N-GDP is 8.4, smaller by almost a factor of 2 compared to the wild type ($T_1/T_2 = 14.2$), suggesting a greater degree of motion of the nucleotide in Cdc42Hs(F28L) compared to that in Cdc42Hs. This is consistent with the 2-fold decrease in NOE for ^{15}N-GDP in Cdc42Hs(F28L) compared to that in the wild type.

Effects of the F28L Mutation on Effector-Binding Regions of Cdc42Hs. The principal aim of this study was to compare the dynamics character of the single-point mutant, Cdc42Hs(F28L), to wild-type Cdc42Hs to determine if the single-point mutation causes local changes in the dynamics at the nucleotide-binding site of the protein or if more global changes in the dynamics of the molecule were apparent that could affect nucleotide exchange and protein function (e.g., changes in effector-binding regions). The dynamics analysis of Cdc42Hs-GDP by Loh et al. (*21*) showed three regions of the molecule with enhanced segmental flexibility with respect to the protein. These regions: (1) Switch I (residues 28−40), (2) Switch II (residues 57−74), and (3) the insert region (residues 122−134) are all involved in protein−protein interactions (*27*, *56*−*59*). Values of ΔS^2 for these regions in Cdc42Hs(F28L) and the wild type are given in Table 4. The dynamics of the Switch II region are very similar in both proteins. As reported by Loh et al. (*21*), the Switch I region is very mobile, resulting in the loss of signal for many Switch I residues because of line broadening. Thus, a comparison of the dynamics in this region for the two proteins is difficult to assess because there is so little information. Of those residues that are detected, residues in the wild type tended to have more complex motions than in Cdc42Hs(F28L), but this may not be representative of the entire switch region.

Although ΔS^2 for the insert region in both proteins is similar in Cdc42Hs(F28L) and the wild type (Table 4), all but two of the insert residues in Cdc42Hs(F28L) fit Model 1; whereas, in the wild type, all but two residues in the insert region fit models that include motions on multiple time scales (models 3−5). Also, several residues in the insert region show much slower H−D exchange than those in the wild

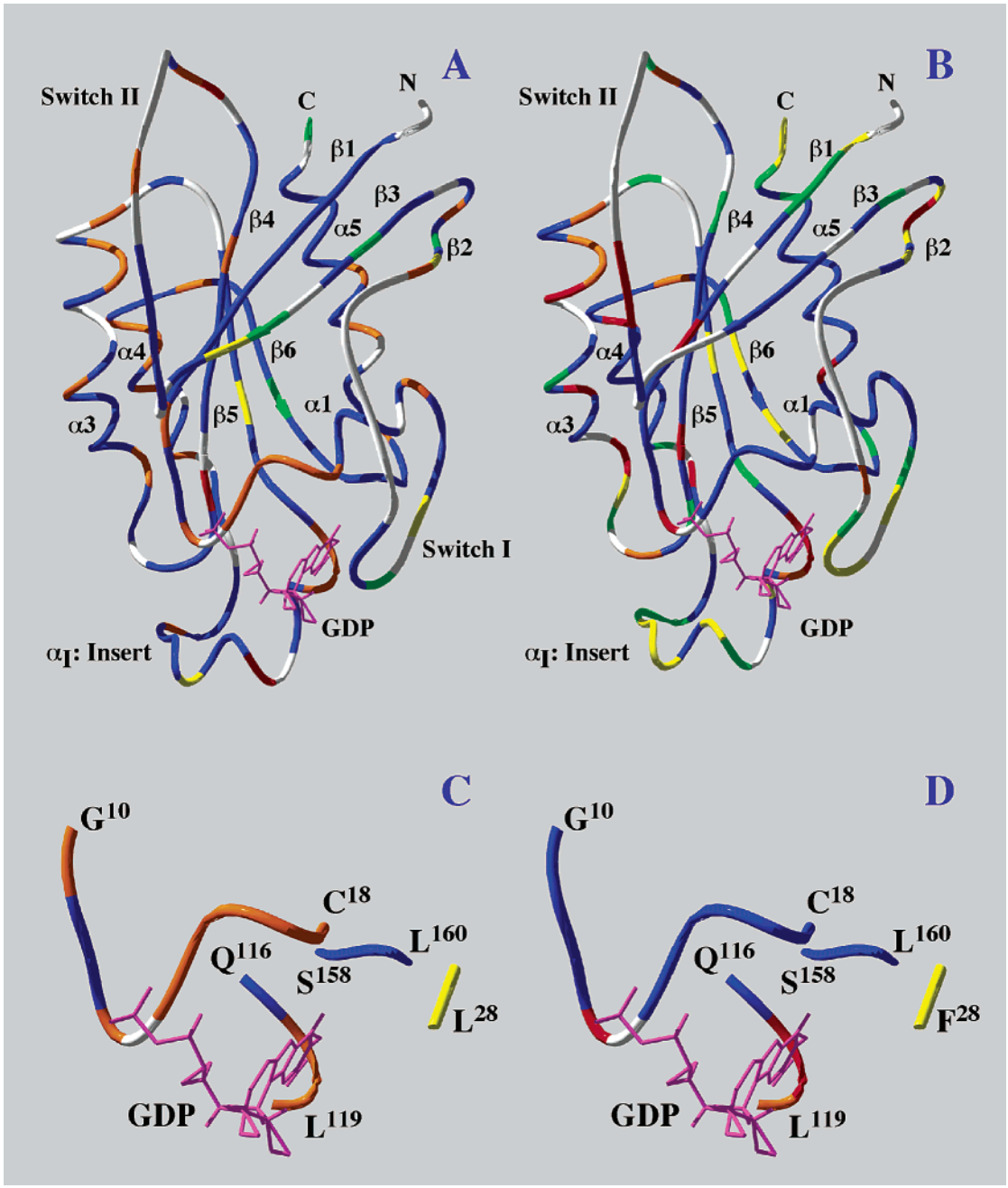

FIGURE 5: Structure of Cdc42Hs-GDP [1AJE (*39*)] colored according to the best-fit dynamics model for (A) Cdc42Hs(F28L) and (B) wild-type Cdc42Hs (*21*). Corresponding expanded views of the nucleotide binding sites are shown in (C) Cdc42Hs(F28L) and (D) wild-type Cdc42Hs. Model assignments are represented as white, unassigned; blue, model 1; green, model 2; orange, model 3; red, model 4; and yellow, model 5. The nucleotide is purple.

type (Figure 2). The removal of the insert region blocks cell transformation by Cdc42Hs(F28L) (*58*), suggesting that it may play a role in the interaction with downstream effectors associated with transformation. Thus, the changes in dynamics in the insert may play a role in this process.

SUMMARY

NMR spectroscopy is an important tool useful in the investigation of protein dynamics because of its sensitivity to motions over a wide range of time scales. From the dynamics analysis of the wild-type protein, the motion in Cdc42Hs can be correlated with the function of the protein, because various types of segmental flexibility may be necessary for regions where effector-binding interactions take place, and this flexibility can be reduced upon binding, for example, binding of p21-activated kinase to Cdc42Hs (*21*). Flexibility can also play a role in substrate binding and catalysis (*32*, *60*). In light of these observations, the dynamics of Cdc42Hs(F28L) foreshadow the importance of motion constriction as it relates to the oncogenic potential of the protein. Just as flexibility in certain locations is important for proper function, so is rigidity in certain locations. For example, the mutation of phenylalanine to leucine at position 28 in Cdc42Hs results in a loss of hydrogen bonding and an increase in the flexibility of the binding site, which ultimately leads to an increased rate of nucleotide dissociation and eventually cell transformation. By characterizing the motions in this oncogenic mutant protein of Cdc42Hs, we have shown

how increasing the flexibility in important ligand-binding regions, without disrupting the conformation of the entire protein, can alter signaling processes.

ACKNOWLEDGMENT

We thank the Laboratory of Chemical Physics at the National Institutes of Health and Drs. Dan Garrett and Frank Delaglio for making available PIPP and NMRPipe, which were useful in analyzing our NMR data. We thank Ahmed Ahmed, Linda Nicholson, and Dawit Gizachew for helpful discussions.

REFERENCES

1. Barbacid, M. (1987) *ras* Genes, *Annu. Rev. Biochem. 56*, 779−827.
2. Bourne, H. R., Sanders, D. A., and McCormick, F. (1991) The GTPase superfamily: Conserved structure and molecular mechanism, *Nature 349*, 117−127.
3. Hart, M. J., Eva, A., Evans, T., Aaronson, S. A., and Cerione, R. A. (1991) Catalysis of guanine nucleotide exchange on the Cdc42Hs protein by the dbl oncogene product, *Nature 354*, 311−314.
4. Horii, Y., Beeler, J. F., Sakaguchi, K., Tachibana, M., and Miki, T. (1994) A novel oncogene, ost, encodes a guanine nucleotide exchange factor that potentially links Rho and Rac signaling pathways, *EMBO J. 13*, 4776−4786.
5. Hart, M. J., Shinjo, K., Hall, A., Evans, T., and Cerione, R. A. (1991) Identification of the human platelet GTPase activating protein for the CDC42Hs protein, *J. Biol. Chem. 266*, 20840−20848.
6. Leonard, D., Hart, M. J., Platko, J. V., Eva, A., Henzel, W., Evans, T., and Cerione, R. A. (1992) The identification and charcterization of a GDP-dissociation inhibitor (GDI) for the CDC42Hs protein, *J. Biol. Chem. 267*, 22860−22868.
7. Bos, J. L. (1989) ras oncogenes in human cancer: A review, *Cancer Res. 49*, 4682−4689.
8. Lin, R., Bagrodia, S., Cerione, R., and Manor, D. (1997) A novel Cdc42Hs mutant induces cellular transformation, *Curr. Biol. 7*, 794−797.
9. Wittinghofer, A., and Pai, E. (1991) The structure of Ras protein: A model for a universal molecular switch, *Trends Biochem. Sci. 16*, 382−387.
10. Saraste, M., Sibbald, P. R., and Wittinghofer, A. (1990) The P-loop−A common motif in ATP- and GTP-binding proteins, *Trends Biochem. Sci. 15*, 430−434.
11. Valencia, A., Kjeldgaard, M., Pai, E. F., and Sander, C. (1991) GTPase domains of ras p21 oncogene protein and elongation factor Tu: Analysis of three-dimensional structures, sequence families, and functional sites, *Proc. Natl. Acad. Sci. U.S.A. 88*, 5443−5447.
12. de Vos, A. M., Tong, L., Milburn, M. V., Matias, P. M., Jancarik, J., Noguchi, S., Nishimura, S., Miura, K., Ohtsuka, E., and Kim, S.-H. (1988) Three-dimensional structure of an oncogene protein: Catalytic domain of human c-H-*ras* p21, *Science 239*, 888−893.
13. Pai, E. F., Kabsch, W., Krengel, U., Holmes, K. C., John, J., and Wittinghofer, A. (1989) Structure of the guanine nucleotide binding domain of the Ha-Ras oncogene product p21 in the triphosphate conformation, *Nature 341*, 209−214.
14. Schlichting, I., Jacob, J., Frech, M., Chardin, P., Wittinghofer, A., Zimmermann, H., and Rosch, P. (1990) Proton NMR studies of transforming and nontransforming H-ras p21 mutants, *Biochemistry 29*, 504−511.
15. John, J., Frech, M., and Wittinghofer, A. (1988) Biochemical properties of Ha-ras encoded p21 mutants and mechanism of the autophosphorylation reaction, *J. Biol. Chem. 263*, 11792−11799.
16. Palmer, A. G., III, Kroenke, C. D., and Loria, J. P. (2001) Nuclear magnetic resonance methods for quantifying microsecond-to-millisecond motions in biological macromolecules, *Methods Enzymol. 339*, 204−238.
17. Forman-Kay, J. D. (1999) The "dynamics" in the thermodynamics of binding, *Nat. Struct. Biol. 6*, 1086−1087.
18. Barthe, P., Chiche, L., Declerck, N., Delsuc, M. A., Lefevre, J. F., Malliavin, T., Mispelter, J., Stern, M. H., Lhoste, J. M., and Roumestand, C. (1999) Refined solution structure and backbone dynamics of 15N-labeled C12A-p8MTCP1 studied by NMR relaxation, *J. Biomol. NMR 15*, 271−288.
19. Gizachew, D., and Oswald, R. E. (2001) Concerted motion of a protein-peptide complex: Backbone dynamics studies of an ^{15}N-labeled peptide derived from P(21)-activated kinase bound to Cdc42Hs.GMPPCP, *Biochemistry 40*, 14368−14375.
20. Kay, L. E. (1998) Protein dynamics from NMR, *Nat. Struct. Biol. 5* (*Suppl.*), 513−517.
21. Loh, A. P., Guo, W., Nicholson, L. K., and Oswald, R. E. (1999) Backbone dynamics of inactive, active, and effector-bound Cdc42Hs from measurements of ^{15}N relaxation parameters at multiple field strengths, *Biochemistry 38*, 12547−12557.
22. Loh, A. P., Pawley, N., Nicholson, L. K., and Oswald, R. E. (2001) An increase in side chain entropy facilitates effector binding: NMR characterization of the side chain methyl group dynamics in Cdc42Hs, *Biochemistry 40*, 4590−4600.
23. Lu, J., Lin, C. L., Tang, C., Ponder, J. W., Kao, J. L., Cistola, D. P., and Li, E. (2000) Binding of retinol induces changes in rat cellular retinol-binding protein II conformation and backbone dynamics, *J. Mol. Biol. 300*, 619−632.
24. Zidek, L., Novotny, M. V., and Stone, M. J. (1999) Increased protein backbone conformational entropy upon hydrophobic ligand binding, *Nat. Struct. Biol. 6*, 1118−1121.
25. Feher, V. A., and Cavanagh, J. (1999) Millisecond-timescale motions contribute to the function of the bacterial response regulator protein Spo0F, *Nature 400*, 289−293.
26. Stock, A. (1999) Biophysics. Relating dynamics to function, *Nature 400*, 221−222.
27. Guo, W., Sutcliffe, M. J., Cerione, R. A., and Oswald, R. E. (1998) Identification of the binding surface on Cdc42Hs for p21-activated kinase, *Biochemistry 37*, 14030−14037.
28. States, D. J., Haberkorn, R. A., and Ruben, D. J. (1982) A Two-dimensional nuclear Overhauser experiment with pure absorption phase in four quadrants, *J. Magn. Reson. 48*, 286−292.
29. Kay, L. E., Keifer, P., and Saarinen, T. (1992) Pure absorption gradient enhanced heteronuclear single quantum correlation spectroscopy with improved sensitivity, *J. Am. Chem. Soc. 114*, 10663−10665.
30. Delaglio, F., Grzesiek, S., Vuister, G. W., Zhu, G., Pfeifer, J., and Bax, A. (1995) NMRPipe: A multidimensional spectral processing system based on UNIX pipes, *J. Biomol. NMR 6*, 277−293.
31. Garrett, D. S., Powers, R., Gronenborn, A. M., and Clore, G. (1991) A common sense approach to peak picking in two-, three-, and four-dimensional spectra using automatic computer analysis of contour diagrams, *J. Magn. Reson. 95*, 214−220.
32. Nicholson, L. K., Yamazaki, T., Torchia, D. A., Grzesiek, S., Bax, A., Stahl, S. J., Kaufman, J. D., Wingfield, P. T., Lam, P. Y., Jadhav, P. K. et al. (1995) Flexibility and function in HIV-1 protease, *Nat. Struct. Biol. 2*, 274−280.
33. Lipari, G., and Szabo, A. (1982) Model-free approach to the interpretation of nuclear magnetic resonance relaxation in macromolecules. 2. Analysis of Experimental Results, *J. Am. Chem. Soc. 104*, 4559−4570.
34. Lipari, G., and Szabo, A. (1982) Model-free approach to the interpretation of nuclear magnetic resonance relaxation in macromolecules. 1. Theory and range of validity, *J. Am. Chem. Soc. 104*, 4546−4559.
35. Clore, G. M., Szabo, A., Bax, A., Kay, L. E., Driscoll, P. C., and Gronenborn, A. M. (1990) Deviations from the simple two-parameter model free approach to the interpretation of ^{15}N nuclear magnetic relaxation of proteins, *J. Am. Chem. Soc. 112*, 4989−4991.
36. Mandel, A. M., Akke, M., and Palmer, A. G., III (1995) Backbone dynamics of *Escherichia coli* ribonuclease HI: Correlations with structure and function in an active enzyme, *J. Mol. Biol. 246*, 144−163.
37. Pawley, N. H., Gans, J. D., and Nicholson, L. K. (2002) Factors determining the reliable description of global tumbling parameters in solution NMR, *J. Biomol. NMR 24*, 215−229.
38. Palmer, A. (1998) *ModelFree*, version 4.0, http://cpmcnet.columbia.edu/dept/gsas/biochem /labs/palmer.
39. Feltham, J. L., Dötsch, V., Raza, S., Manor, D., Cerione, R. A., Sutcliffe, M. J., Wagner, G., and Oswald, R. E. (1997) Definition of the switch surface in the solution structure of Cdc42Hs, *Biochemistry 36*, 8755−8766.

40. Kay, L. E., Torchia, D. A., and Bax, A. (1989) Backbone dynamics of proteins as studied by ^{15}N inverse detected heteronuclear NMR spectroscopy: Application to staphylococcal nuclease, *Biochemistry 28*, 8972−8979.
41. Nicholson, L. K., Kay, L. E., Baldisseri, D. M., Arango, J., Young, P. E., Bax, A., and Torchia, D. A. (1992) Dynamics of methyl groups in proteins as studied by proton-detected ^{13}C NMR spectroscopy, *Biochemistry 31*, 5253−5263.
42. Tong, L., de Vos, A. M., Milburn, M. V., Jancarik, J., Noguchi, S., Nishimura, S., Miura, K., Ohtsuka, E., and Kim, S.-H. (1989) Structural differences between a ras oncogene protein and the normal protein, *Nature 337*, 90−93.
43. Krengel, U., Schlichting, I., Scherer, A., Schumann, R., Frech, M., John, J., Kabsch, W., Pai, E. F., and Wittinghofer, A. (1990) Three-dimensional structures of H-ras p21 mutants: Molecular basis for their inability to function as signal switch molecules, *Cell 62*, 539−548.
44. Hoffman, G. R., Nassar, N., and Cerione, R. A. (2000) Structure of the rho family GTP-binding protein Cdc42 in complex with the multifunctional regulator RhoGDI, *Cell 100*, 345−356.
45. Hirshberg, M., Stockley, R. W., Dodson, G., and Webb, M. R. (1997) The crystal structure of human rac1, a member of the rho-family complexed with a GTP analogue, *Nat. Struct. Biol. 4*, 147−152.
46. Tong, L., de Vos, A. M., Milburn, M. V., and Kim, S.-H. (1991) Crystal structures at 2.2 Å resolution of the catalytic domains of normal *ras* protein and an oncogenic mutant complexed with GDP, *J. Mol. Biol. 217*, 503−516.
47. Wei, Y., Zhang, Y., Derewenda, U., Liu, X., Minor, W., Nakamoto, R. K., Somlyo, A. V., Somlyo, A. P., and Derewenda, Z. S. (1997) Crystal structure of rhoA-GDP and its functional implications, *Nat. Struct. Biol. 4*, 699−703.
48. Pai, E. F., Krengel, U., Petsko, G. A., Goody, R. S., Kabsch, W., and Wittinghofer, A. (1990) Refined crystal structure of the triphosphate conformation of H-ras p21 at 1.35 Å resolution: Implication for the mechanism of GTP hydrolysis, *EMBO J. 9*, 2351−2359.
49. Seeburg, P. H., Colby, W. W., Capon, D. J., Goeddel, D. V., and Levinson, A. K. (1984) Biological properties of human c-Ha-*ras* 1 genes mutated at codon 12, *Nature 312*, 71−75.
50. Qiu, R. G., Abo, A., McCormick, F., and Symons, M. (1997) Cdc42 regulates anchorage-independent growth and is necessary for Ras transformation, *Mol. Cell. Biol. 17*, 3449−3458.
51. Rudolph, M. G., Wittinghofer, A., and Vetter, I. R. (1999) Nucleotide binding to the G12V-mutant of Cdc42 investigated by X-ray diffraction and fluorescence spectroscopy: Two different nucleotide states in one crystal, *Protein Sci. 8*, 778−787.
52. Miller, A.-F., Papastavros, M. Z., and Redfield, A. G. (1992) NMR studies of the conformational change in human N-p21^{ras} produced by replacement of bound GDP with the GTP analog GTPγS, *Biochemistry 31*, 10208−10216.
53. Redfield, A. G., and Papastavros, M. Z. (1990) NMR study of the phosphoryl binding loop in purine nucleotide proteins: Evidence for strong hydrogen bonding in human N-ras p21, *Biochemistry 29*, 3509−3514.
54. Wüthrich, K. (1986) *NMR of Proteins and Nucleic Acids*, John Wiley and Sons, New York.
55. Clore, G. M., Driscoll, P. C., Wingfield, P. T., and Gronenborn, A. M. (1990) Analysis of the backbone dynamics of interleukin-1 β using two-dimensional inverse detected heteronuclear ^{15}N-^{1}H NMR spectroscopy, *Biochemistry 29*, 7387−7401.
56. Rittinger, K., Walker, P. A., Eccleston, J. F., Nurmahomed, K., Owen, D., Laue, E., Gamblin, S. J., and Smerdon, S. J. (1997) Crystal structure of a small G protein in complex with the GTPase-activating protein rhoGAP, *Nature 388*, 693−607.
57. Nassar, N., Hoffman, G. R., Manor, D., Clardy, J. C., and Cerione, R. A. (1998) Structures of Cdc42 bound to the active and catalytically compromised forms of Cdc42GAP, *Nat. Struct. Biol. 5*, 1047−1052.
58. Wu, W. J., Lin, R., Cerione, R. A., and Manor, D. (1998) Transformation activity of Cdc42 requires a region unique to Rho-related proteins, *J. Biol. Chem. 273*, 16655−16658.
59. Gizachew, D., Guo, W., Chohan, K. K., Sutcliffe, M. J., and Oswald, R. E. (2000) Structure of the complex of Cdc42Hs with a peptide derived from P-21 activated kinase, *Biochemistry 39*, 3963−3971.
60. Luque, I., and Freire, E. (2000) Structural stability of binding sites: Consequences for binding affinity and allosteric effects, *Proteins Suppl.* 63−71.

BI0490901